ORIGINAL ARTICLE

Reference data and calculators for second-generation HR-pQCT measures of the radius and tibia at anatomically standardized regions in White adults

S. J. Warden[1,2] · Z. Liu[2,3] · R. K. Fuchs[1,2] · B. van Rietbergen[4] · S. M. Moe[2,5]

Abstract

Summary High-resolution peripheral quantitative computed tomography (HR-pQCT) is a powerful tool to assess bone health. To determine how an individual's or population of interest's HR-pQCT outcomes compare to expected, reference data are required. This study provides reference data for HR-pQCT measures acquired in a population of White adults.

Purpose To provide age- and sex-specific reference data for high-resolution peripheral quantitative computed tomography (HR-pQCT) measures of the distal and diaphyseal radius and tibia acquired using a second-generation scanner and percent-of-length offsets proximal from the end of the bone.

Methods Data were acquired in White adults (aged 18–80 years) living in the Midwest region of the USA. HR-pQCT scans were performed at the 4% distal radius, 30% diaphyseal radius, 7.3% distal tibia, and 30% diaphyseal tibia. Centile curves were fit to the data using the LMS approach.

Results Scans of 867 females and 317 males were included. The fitted centile curves reveal HR-pQCT differences between ages, sexes, and sites. They also indicate differences when compared to data obtained by others using fixed length offsets. Excel-based calculators based on the current data were developed and are provided to enable computation of subject-specific percentiles, z-scores, and t-scores and to plot an individual's outcomes on the fitted curves. In addition, regression equations are provided to convert estimated failure load acquired with the conventional criteria utilized with first-generation scanners and those specifically developed for second-generation scanners.

Conclusion The current study provides unique data and resources. The combination of the reference data and calculators provide clinicians and investigators an ability to assess HR-pQCT outcomes in an individual or population of interest, when using the described scanning and analysis procedure. Ultimately, the expectation is these data will be expanded over time so the wealth of information HR-pQCT provides becomes increasingly interpretable and utilized.

Keywords Bone strength · Centile curves · High-resolution peripheral quantitative computed tomography · Microarchitecture · Reference values

✉ S. J. Warden
stwarden@iu.edu

1 Department of Physical Therapy, School of Health and Human Sciences, Indiana University, 1140 W. Michigan St., CF-120, Indianapolis, IN 46202, USA

2 Indiana Center for Musculoskeletal Health, Indiana University, Indianapolis, IN, USA

3 Department of Biostatistics, School of Medicine, Indiana University, Indianapolis, IN, USA

4 Department of Biomedical Engineering, Eindhoven University of Technology, Eindhoven, The Netherlands

5 Division of Nephrology, Department of Medicine, School of Medicine, Indiana University, Indianapolis, IN, USA

Introduction

High-resolution peripheral quantitative computed tomography (HR-pQCT) is a powerful clinical research tool providing non-invasive measures of bone microarchitecture as well as micro-finite element (μFE) estimates of bone strength. Bone strength estimates from HR-pQCT data predict incident fracture and improve fracture prediction beyond femoral neck areal bone mineral density (BMD) or fracture risk assessment tool (FRAX) scores alone [1, 2]. These findings suggest utility of HR-pQCT in fracture prediction; however, its use in the clinical realm is limited due to a lack of

instrument availability, comparatively high data acquisition burden, and limited availability of reference data.

A number of studies have provided reference data for HR-pQCT outcomes [3–17]. These provide a means of expressing an individual's outcomes relative to peers, including adolescents and young adults [6, 8], and adults from a range of racial and ethnic backgrounds [3–5, 7, 9–17]. However, the majority of studies [3–12, 14, 17] utilized data acquired with the first-generation HR-pQCT scanner, which had nominal isotropic resolution (82 μm) and required derivation of trabecular microarchitecture based on assumptions about tissue density. The more recently introduced second-generation HR-pQCT scanner has provided enhanced spatial resolution (61 μm) and allows for direct voxel-based measures of trabecular microarchitecture [18]. In addition, the second-generation scanner has a larger scan length in the axial direction enabling greater access to proximal scan positions. Assessment of cortical bone-rich diaphyseal sites may provide unique insight into cortical bone changes with aging, disease, and lifestyle and pharmaceutical interventions.

Preliminary studies have provided reference data for outcomes acquired at distal bone sites with the second-generation HR-pQCT scanner [13, 15, 16]. However, as with the previous studies using the first-generation scanner [3–7, 9–12, 14, 17], scan locations were offset a fixed distance proximal from the end of the respective bone (typically 9.5 mm [first-generation HRpQCT] or 9.0 mm [second-generation] for the distal radius and 22.5 mm [first-generation] or 22.0 mm [second-generation] for the distal tibia). Scanning at a fixed offset can lead to the introduction of systematic bias in cross-sectional comparisons as it does not account for the impact of bone length [19–21]. For example, scanning at a fixed offset in an individual with shorter bone lengths causes the volume of interest to be more proximal. The result is a systematically smaller bone size, with elevated density due to the inclusion of more cortical and less trabecular bone [22].

To address the impact of bone length on HR-pQCT outcomes and enable assessment of anatomically similar regions between individuals, the recommendation is to position volumes of interest relative to a percent offset of bone length [23]. To our knowledge, only one reference data set performed scans using percent-of-length offsets, but the data were acquired using a first-generation scanner and limited to adolescents and young adults [8]. Also, no study that we are aware of has provided reference data for scans performed at proximal/diaphyseal bone sites.

The primary purpose of the current study was to generate age- and sex-specific normative data for HR-pQCT measures of the distal and diaphyseal radius and tibia across adulthood using a second-generation scanner and percent-of-length offsets. A secondary objective was to generate regression equations to convert between μFE-estimated failure load using criteria conventionally utilized with first-generation HR-pQCT

scanners ("Pistoia criteria") [24], but still being used with second-generation scanners [15, 16], and those specifically developed for the different scan volume and resolution of second-generation HR-pQCT scanners ("Arias-Morena criteria") [25]. Using the cumulative data, the ultimate goal of the study was to provide researchers and clinicians with practical Microsoft Office Excel-based calculators to compute subject-specific percentiles, z-scores, and t-scores for each outcome and plot outcomes on centile curves.

Methods

Participants

HR-pQCT scans were performed on 1,598 adults (aged ≥ 18 years) between 12/2017 and 6/2021 within the Musculoskeletal Function, Imaging, and Tissue (MSK-FIT) Resource Core of the Indiana Center for Musculoskeletal Health's Clinical Research Center (Indianapolis, IN). Participants were recruited to the core by investigators seeking standardized musculoskeletal outcomes for their research subjects, as well as from the local community via self-referral from posted flyers, word-of-mouth, an online research volunteer registry (https://research.indianactsi.org/volunteers/registration/), and community presentations. The MSK-FIT core has Institutional Review Board approval from Indiana University to assess all-comers who provide written informed consent.

To be eligible for inclusion in the current dataset, participants were required to (1) be between 18 and 80 years of age; (2) self-identify as being of White ancestry; (3) be ambulatory; and (4) have no self-reported diabetes, liver or kidney disease, past or present history of cancer, thyroid disorders, cystic fibrosis, or rare bone disease. Individuals with the later conditions were excluded due to their known or potential impact on HR-pQCT outcomes [26] and their over-representation in the MSK-FIT Resource Core cohort resulting from investigator-initiated trials. An upper age limit of 80 years was selected because the MSK-FIT Resource Core cohort currently has a limited number of participants beyond this age, with centile curves being sensitive to low numbers of individuals at the tail of distributions. Individuals with osteoporosis were included if they were not currently taking bone active therapies. There was no criterion regarding the timing of the last dose in individuals with a history of taking these therapies.

Participant characteristics

Height (to the nearest 0.1 cm) and weight (to the nearest 0.1 kg) were measured without shoes using a calibrated

stadiometer (Seca 264; Seca GmbH & Co., Hamburg, Germany) and scale (MS140-300; Brecknell, Fairmont, MN), respectively. Appendicular skeletal muscle mass relative to height (ASM/height^2; kg/m^2) and whole-body aBMD were assessed by whole-body dual-energy x-ray absorptiometry (DXA) (Norland Elite; Norland at Swissray, Fort Atkinson, WI). Regional DXA using the same scanner assessed total hip and spine aBMD to determine osteoporosis status.

High-resolution peripheral quantitative computed tomography (HR-pQCT)

HR-pQCT (XtremeCT II; Scanco Medical, Bruttisellen, Switzerland) was used to image participants' non-dominant arm and leg. Scanner stability throughout the duration of data collection was confirmed by scanning phantoms with inserts of known density and volume, as per manufacturer instructions. The non-dominant leg was defined as the leg contralateral to the participants' non-dominant arm, as per the concept of crossed symmetry [27, 28]. Bone length was

Table 1 Participant characteristics stratified by decade of age[†]

Characteristic	Age group (years)					
	18–29	30–39	40–49	50–59	60–69	70–80
Females						
n	161	98	111	189	232	76
Height (m)	1.65 (1.61–1.70)	1.65 (1.62–1.70)	1.65 (1.61–1.69)	1.64 (1.60–1.67)	1.62 (1.59–1.67)	1.62 (1.59–1.65)
Ulna length (cm)	25.6 (24.7–26.5)	25.3 (24.6–26.2)	25.3 (24.7–26.3)	25.3 (24.5–26.2)	25.2 (24.4–26.0)	25.1 (24.6–25.9)
Tibia length (cm)	37.0 (35.6–38.4)	36.8 (35.7–37.9)	36.7 (34.9–38.1)	36.9 (35.5–38.0)	36.7 (35.4–38.1)	36.6 (35.1–38.1)
Weight (kg)	67.2 (59.0–76.1)	67.6 (60.5–80.1)	73.1 (60.5–86.9)	70.7 (60.6–83.2)	70.0 (61.9–81.4)	65.8 (59.7–76.8)
BMI (kg/m^2)	24.6 (21.7–27.8)	24.1 (21.7–29.8)	26.1 (22.4–33.0)	26.0 (22.6–31.4)	26.2 (23.0–31.1)	25.6 (22.6–29.0)
ASM/height (kg/m^2)	7.58 (6.75–8.45)	7.44 (6.69–8.11)	7.52 (6.78–8.12)	6.96 (6.38–8.04)	6.94 (6.36–7.61)	6.47 (5.98–7.18)
Whole-body aBMD (g/cm^2)	0.93 (0.85–0.99)	0.92 (0.85–0.98)	0.92 (0.84–0.97)	0.85 (0.79–0.91)	0.83 (0.77–0.89)	0.83 (0.77–0.87)
Total hip aBMD (g/cm^2)	1.05 (0.96–1.15)	1.02 (0.94–1.10)	0.98 (0.87–1.08)	0.89 (0.79–0.98)	0.83 (0.77–0.91)	0.82 (0.78–0.91)
Spine aBMD (g/cm^2)	1.14 (1.02–1.22)	1.11 (1.05–1.22)	1.10 (0.97–1.24)	0.98 (0.88–1.10)	0.99 (0.87–1.12)	1.04 (0.92–1.21)
HR-pQCT scans included (*n*)						
Distal radius	153	93	109	184	224	68
Radial diaphysis	159	97	108	189	226	71
Distal tibia	137	90	103	158	201	64
Tibial diaphysis	136	89	100	160	200	63
Males						
n	91	38	26	36	80	46
Height (m)	1.78 (1.74–1.83)	1.77 (1.73–1.81)	1.77 (1.73–1.85)	1.76 (1.71–1.83)	1.78 (1.74–1.81)	1.74 (1.70–1.78)
Ulna length (cm)	28.3 (27.1–28.9)	27.8 (26.7–28.8)	28.0 (26.9–29.0)	28.1 (27.0–29.0)	28.1 (27.0–29.4)	27.8 (27.1–29.1)
Tibia length (cm)	40.1 (39.1–41.9)	39.3 (38.1–40.7)	39.7 (37.7–43.4)	39.6 (37.9–41.3)	40.0 (38.5–41.5)	39.3 (38.2–40.6)
Weight (kg)	80.8 (72.8–91.3)	83.8 (77.9–96.5)	90.5 (80.8–97.3)	82.1 (76.4–96.1)	84.2 (75.6–96.4)	85.5 (76.2–94.5)
BMI (kg/m^2)	25.0 (23.4–28.3)	26.5 (24.9–31.3)	28.2 (25.3–30.6)	27.1 (24.5–32.3)	26.7 (24.1–29.7)	28.3 (24.9–30.3)
ASM/height (kg/m^2)	9.42 (8.78–10.31)	9.68 (8.97–10.18)	9.29 (8.59–10.66)	8.92 (8.34–9.97)	8.49 (8.02–9.50)	8.27 (7.63–8.85)
Whole-body aBMD (g/cm^2)	1.05 (0.98–1.12)	1.03 (0.95–1.10)	1.00 (0.97–1.12)	1.01 (0.92–1.09)	1.01 (0.94–1.10)	0.98 (0.91–1.02)
Total hip aBMD (g/cm^2)	1.12 (1.01–1.26)	1.10 (0.94–1.15)	1.02 (0.93–1.09)	0.98 (0.88–1.09)	0.96 (0.87–1.08)	0.92 (0.83–0.96)
Spine aBMD (g/cm^2)	1.14 (1.02–1.23)	1.06 (0.98–1.17)	1.08 (0.98–1.27)	1.07 (0.97–1.25)	1.23 (1.05–1.36)	1.15 (1.06–1.31)
HR-pQCT scans included (*n*)						
Distal radius	89	38	26	34	79	44
Radial diaphysis	90	35	22	33	78	44
Distal tibia	80	35	24	33	71	40
Tibial diaphysis	70	31	21	30	61	35

ASM appendicular skeletal muscle mass, *BMI* body mass index

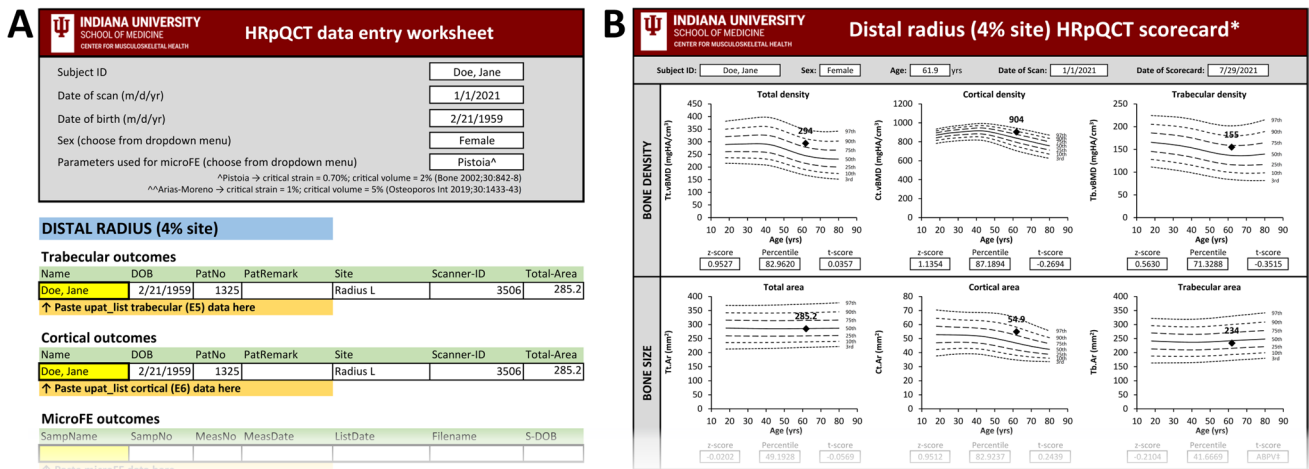[†]Data are median (interquartile range), except for frequencies

Fig. 1 Screenshots of the Excel-based calculator for the radius available in Supplemental file 1. Following entry of basic demographic information and one or more HRpQCT outcome (**A**), subject-specific percentiles, z-scores, and t-scores are computed, and centile curves plotted (**B**)

measured in triplicate using a segmometer (Realmet Flexible Segmometer, NutriActiva, Minneapolis, MN) and as described by Bonaretti et al. [19]. Per convention, ulna length was measured as a surrogate for radial length. The skin overlying the distal apex of the subject's ulnar styloid was marked

and the subject's elbow placed on a rigid surface. The distance between the surface and styloid mark was measured. Tibial length was measured as the distance between skin marks placed at the distal tip of the medial malleolus and the medial joint line of the knee. Short-term precision for

Fig. 2 Representative HRpQCT images of the distal radius and tibia and radial and tibial diaphyses in young (18–20 years) and older (75–80 years) females. Scans were chosen based on failure load (using Pistoia criteria) being within ±2% of the respective percentile (10th, 50th, and 90th)
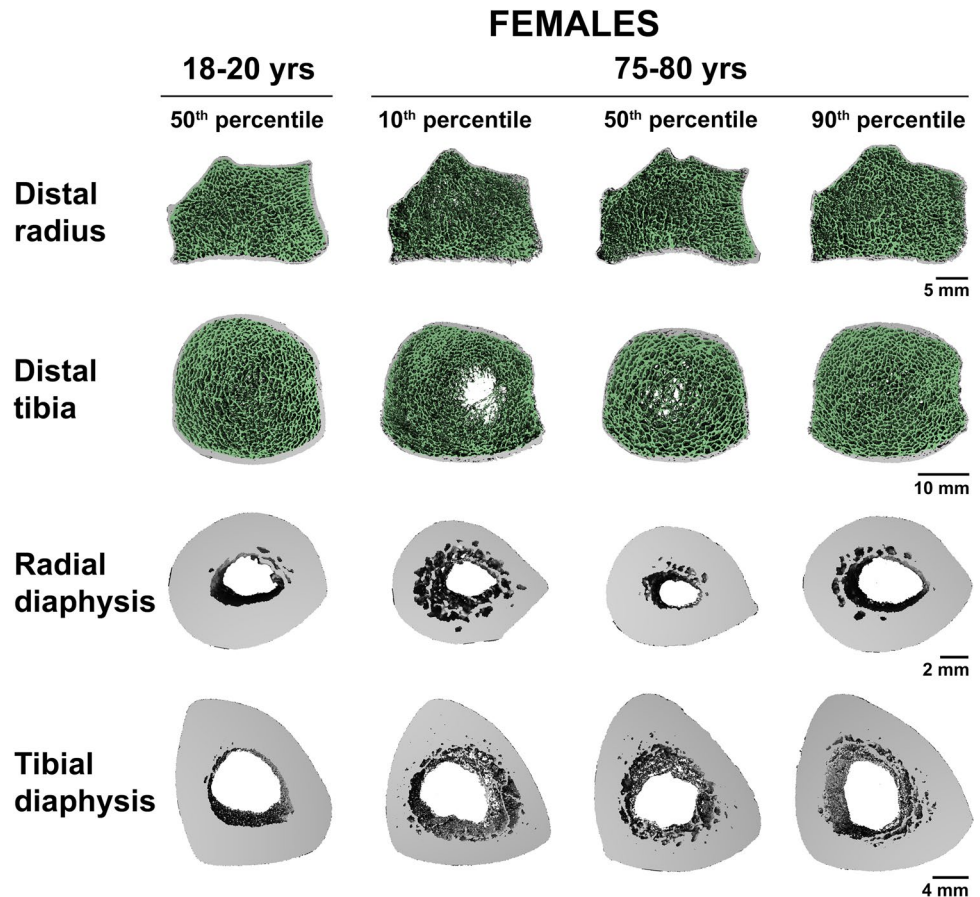
repeat mark placement and length measures of the ulna and tibia in 15 individuals tested on two consecutive days showed root mean square standard deviations of 2.8 mm (1.1%) and 6.3 mm (1.7%), respectively.

Scans were acquired as previously described [29] by one of three similarly trained operators. Subjects laid supine on a moveable treatment plinth and the limb to be imaged immobilized using a padded, anatomically formed carbon fiber cast. The scanner operated at 68 kVp and 1.47 mA to acquire 168 slices (10.2 mm of bone length) with a voxel size of 60.7 μm. After performance of scout scans, reference lines were placed at the medial edge of the distal radius articular surface and center of the tibia joint surface [23]. Scan stacks were centered 4% and 30% of bone length proximal to the radius reference line and 7.3% and 30% of bone length proximal to the tibia reference line, as recommended when employing the percent-of-length offset approach [23]. Scans were scored for motion artifacts on a standard scale of 1 (no motion) to 5 (significant blurring of the periosteal surface, discontinuities in the cortical shell) [30]. Scans scoring ≥ 3 were repeated when time permitted. Scans with a motion artifact of 4 or 5 were excluded from analyses.

Reconstructed images were analyzed according to the manufacturer's standard protocol. The outer periosteal and inner endosteal surfaces of the bone were identified automatically, and segmentations checked for accuracy and manually modified when needed. To assess microarchitectural outcomes, images were filtered using a low-pass Gaussian filter (sigma 0.8, support 1.0 voxel) and fixed thresholds used to extract trabecular and cortical bone (320 and 450 mgHA/cm^3, respectively).

The following outcomes were recorded at distal sites: total vBMD (Tt.vBMD, mgHA/cm^3) and area (Tt.Ar, mm^2); trabecular vBMD (Tb.vBMD, mgHA/cm^3), area (Tb.Ar, mm^2), bone volume/total volume (Tb.BV/TV, %), thickness (Tb.Th, mm), number (Tb.N, 1/mm), and separation (mm); and cortical vBMD (Ct.vBMD, mgHA/cm^3), area (Ct. Ar, mm^2), thickness (Ct.Th, mm), porosity (Ct.Po, %), and porosity diameter (Ct.Po.Dm, mm). The following outcomes were measured at diaphyseal sites: Tt.Ar (mm^2), Ct.vBMD (mgHA/cm^3), Ct.Ar (mm^2), Ct.Th (mm), Ct.Po (%), and Ct.Po.Dm (mm).

μFE analysis (Scanco Medical FE software version 1.13) was used to estimate stiffness (kN/mm) and failure load (N) at both the distal and diaphyseal sites. Each voxel within the segmented HR-pQCT images was assigned a modulus of 10 GPa and Poisson's ratio of 0.3 [24]. Axial compression was applied and failure load estimated using two sets of criteria. The first set ("Pistoia criteria") were

Fig. 3 Representative HRpQCT images of the distal radius and tibia and radial and tibial diaphyses in young (18–20 years) and older (75–80 years) males. Scans were chosen based on failure load (using Pistoia criteria) being within ± 2% of the respective percentile (10th, 50th, and 90th)
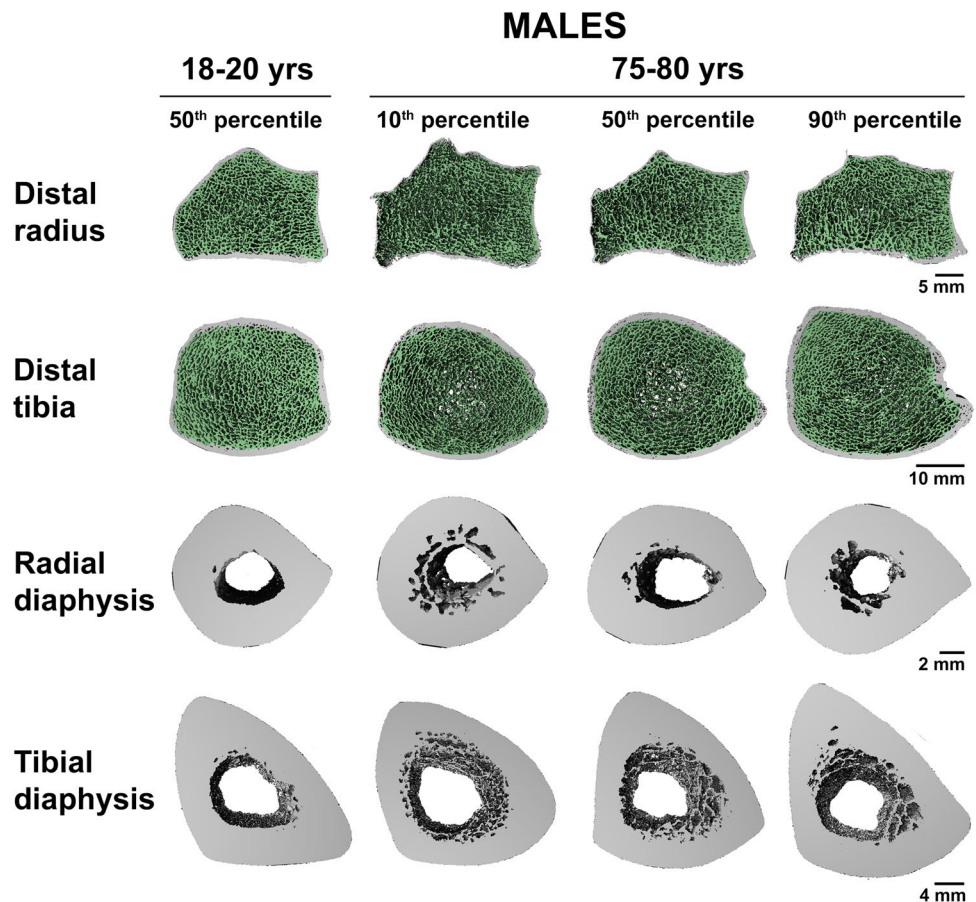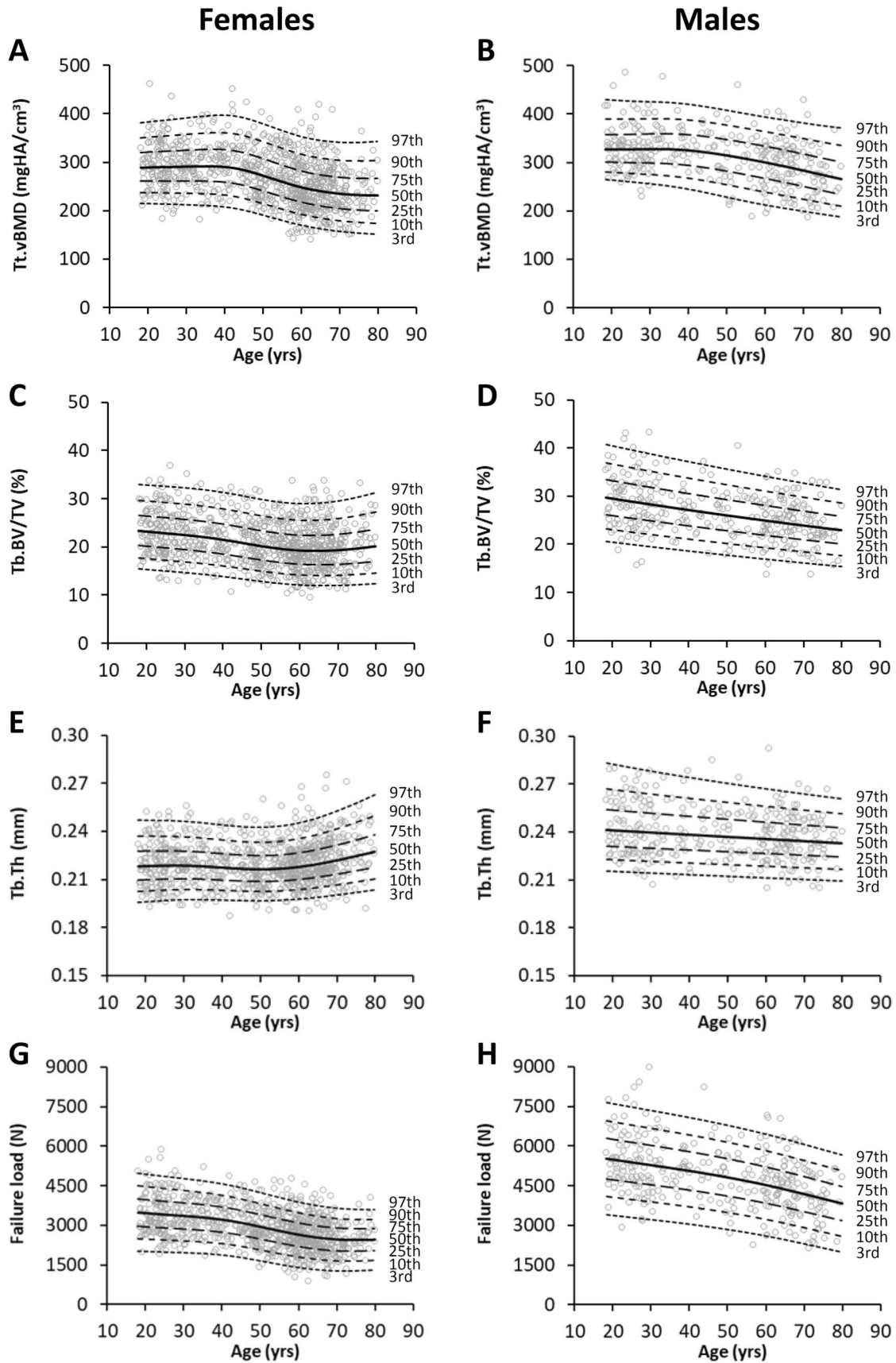
DISTAL RADIUS

Females   Males

◀**Fig. 4** Centile curves for Tt.vBMD (**A**,**B**), Tb.BV/TV (**C**,**D**), Tb.Th (**E**,**F**), and estimated failure load (using Pistoria criteria) (**G**,**H**) at the distal radius for females and males using a 4% percent-of-length offset

those conventionally utilized with first-generation HR-pQCT scanners and estimated failure load when 2% of elements exceeded 0.7% strain [24]. The second set of criteria ("Arias-Morena criteria") were developed for the different scan volume and resolution of second-generation HR-pQCT scanners and estimated failure load when 5% of elements exceeded 1% strain [25].

Short-term precision on duplicate scans with repositioning, but using the initially obtained limb length, in 15 individuals showed root mean square coefficients of variation (RMS-CV) of $< 0.6\%$ for bone density (Tt.vBMD, Ct.vBMD, Tb.vBMD) and $< 0.8\%$ for bone size (Tt.Ar, Ct.Ar, Tb.Ar) at both distal and diaphyseal sites and 1.8–2.9% and $< 1\%$ for estimated failure load at distal and diaphyseal sites, respectively. RMS-CVs for trabecular microarchitecture outcomes (Tb.BV/TV, Tb.N, Tb.Th, Tb.Sp) at distal sites were 0.7–3.2%, whereas for Ct.Po they were 10.3–15.4% and 4.6–6.7% at distal and diaphyseal sites, respectively. The impact of a second measure of limb length prior to repositioning on precision was not assessed.

Statistical analyses

All statistical analyses were performed for females and males separately. Sex-specific participant characteristics were described according to decade stage of life (18–29, 30–39, 40–49, 50–59, 60–69, and 70–80 years). Categorical variables were summarized by frequencies. Continuous variables were summarized by medians and interquartile ranges. After checking assumptions of normality, linearity, homoscedasticity, and absence of collinearity using IBM SPSS Statistics (v27; IBM Corporation, Armonk, NY), linear regression was used to model the relationship between the two sets of criteria (Pistoia and Arias-Morena) for estimating failure load.

Sex-specific reference centile curves for each outcome were generated using the LMS method [31] with R package GAMLSS (version 5.2.0) [32]. The LMS method uses Box-Cox transformation to achieve normality at a given age (Box-Cox Cole and Green [BCCG] distribution). Nonparametric smooth curves are fit to the parameter values across the age range using penalized likelihood with penalty on the second derivatives. Additionally, non-negativity of biological measurements is incorporated by adopting truncated normal distributions, where the truncations are negligible in most cases.

The GAMLSS package provides more flexibilities other than normal and BCCG distributions. Additional distributions include Box-Cox power exponential (BCPE) and Box-Cox t (BCT), which model kurtosis in addition to the skewness modeled by BCCG. We used Akaike information criterion (AIC) to compare the different possible models and determine which best fit the data. However, we report results solely based on BCCG (and normal) distributions for reasons detailed in the results section.

Centile curves, z-scores, and t-scores were calculated from the estimated parameter curves. As per convention, z-scores represent the number of standard deviations the subject-specific outcome varies from age- and sex-matched median outcomes, whereas t-scores represent the number of standard deviations the subject-specific outcome varies from the best sex-specific median outcome. The age when peak outcome was achieved was determined as the highest point on the fitted median curve. Ct.Po, Ct.Po.Dm, and Tb.Sp were exceptions as lower values were considered more desirable. Peak for these outcomes was the lowest point on the median curve.

Because the LMS transformation method to achieve normality constrains maximum obtainable z- and t-scores, LMS-derived z- and t-scores are not suited for identifying extreme values. To address this, modified z- and t-scores are provided for scores greater than $+2$. In modified z-scores, the HR-pQCT outcome is expressed relative to the sex- and age-matched median in units of half the distance between 0 and $+2$ z-scores, as per the approach used for growth charts [33]. Modified t-scores are expressed in units half the distance between 0 and $+2$ z-scores at the age of best sex-specific median outcome in the database.

Results

Participant and scan characteristics

A total of 1,184 participants (867 females, 317 males) were included (Table 1). The sex discrepancy resulted from the self-referral pattern of local community members volunteering to be tested. Reasons for exclusion included (1) age > 80 years ($n = 25$); (2) race not White ($n = 226$); and (3) self-reported ineligible disease or illness ($n = 163$). The final cohort included females and males ranging in age from 18.0 to 79.9 years and 18.4 to 80.0 years, respectively. Total hip and/or spine aBMD t-score was -1 to -2.5 and ≤ -2.5 in 252 (29.1%) and 20 (2.3%) females, respectively. One hundred eight (34.1%) and 21 (6.6%) males had a total hip and/or spine aBMD t-score -1 to -2.5 and < -2.5, respectively.
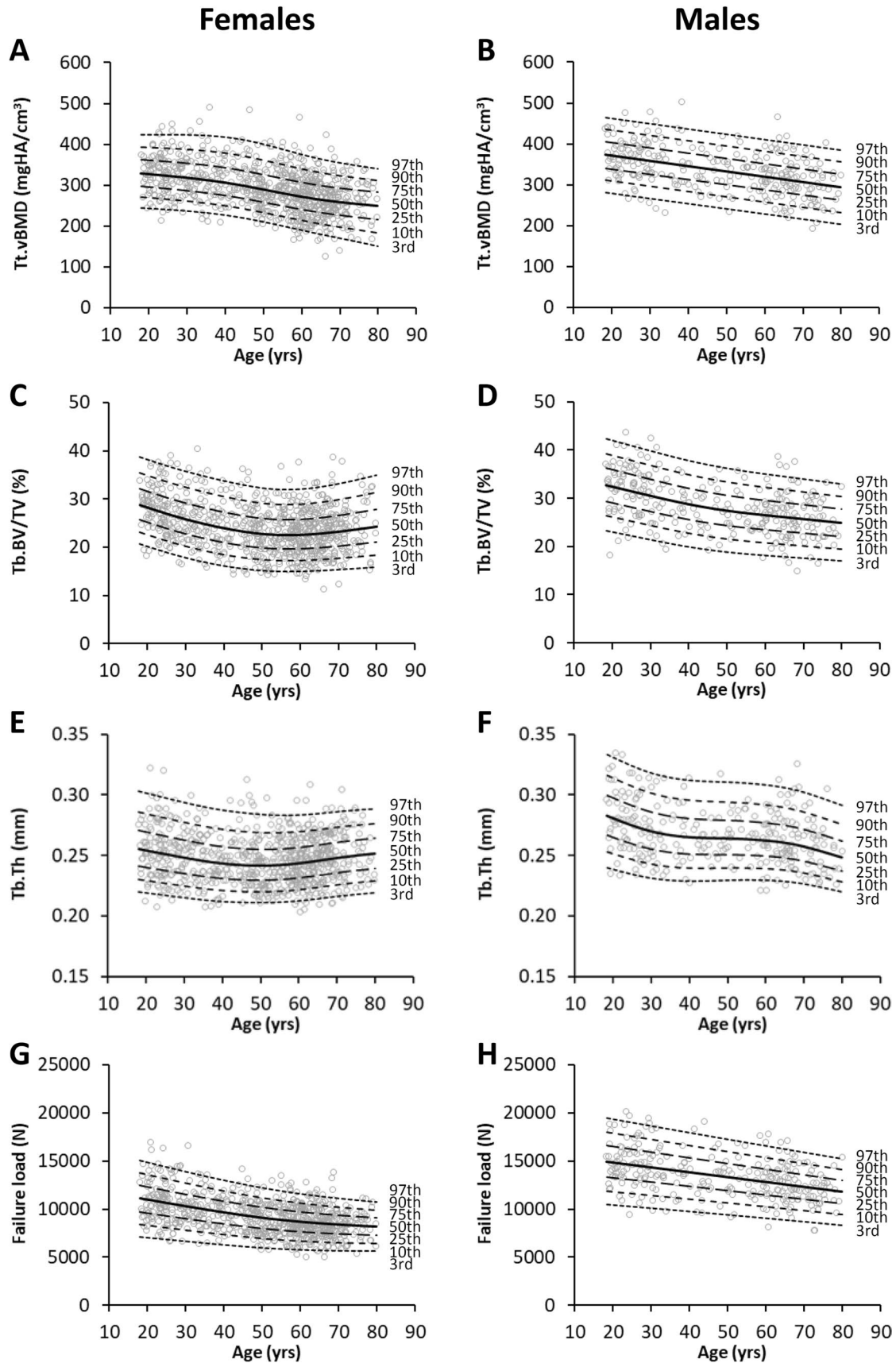
DISTAL TIBIA

◄**Fig. 5** Centile curves for Tt.vBMD (**A,B**), Tb.BV/TV (**C,D**), Tb.Th (**E,F**), and estimated failure load (using Pistoria criteria) (**G,H**) at the distal tibia for females and males using a 7.3% percent-of-length offset

HR-pQCT reference data in females was generated from 831, 850, 753, and 748 scans of the distal radius, radial diaphysis, distal tibia, and tibial diaphysis, respectively. Lower scan numbers than participants was due to: (1) scan not performed due to a lack of subject time ($n = 10$, 10, 64, and 67 participants at the distal radius, radial diaphysis, distal tibia, and tibial diaphysis, respectively); (2) participant too large for the carbon fiber cast or presence of a local tomography artifact on the scan due to the limb being too large and absorbing tissue being outside of field of view ($n = 30$ and 39 participants at the distal tibia and tibial diaphysis, respectively); and (3) excessive motion artifact ($n = 26$, 7, 20, and 13 scans at the distal radius, radial diaphysis, distal tibia, and tibial diaphysis, respectively).

Male HR-pQCT reference data was generated from 310, 302, 283, and 248 scans of the distal radius, radial diaphysis, distal tibia, and tibial diaphysis, respectively. Less scans than participants was due to: (1) scan not performed ($n = 10$, 23, and 33 participants at the radial diaphysis, distal tibia, and tibial diaphysis, respectively); (2) participant too large for the carbon fiber cast or presence of a local tomography artifact on the scan due to the limb being too large and absorbing tissue being outside of field of view ($n = 8$ and 24 participants at the distal tibia and tibial diaphysis, respectively); and (3) excessive motion artifact ($n = 7$, 5, 3, and 12 scans at the distal radius, radial diaphysis, distal tibia, and tibial diaphysis, respectively).

Percentile, z-score, and t-score calculator, and centile curve plotter

Excel calculators based on the normative curves fitted using the LMS approach were developed for both distal and diaphyseal scan locations within the radius (Supplemental file 1) and tibia (Supplemental file 2). The AIC procedure indicated BCCG or normal distributions best fit the data for 34 and 35 of the variables in females and males, respectively (Supplemental file 3). BCPE or BCT best fit the data for the other 16 and 15 variables in females and males, respectively. We solely report results based on BCCG and normal as: (1) the estimated centiles were very similar regardless of the AIC differences; (2) the kurtosis modeled by BCPE or BCT presents only in the extreme tails of distributions and, as such, affects the distribution only beyond the 1st and 99th centiles [34]; and (3) we wanted to use Excel to create downloadable normative data calculators. It is straightforward to incorporate either BCCG or normal distributions in Excel using built-in

functions, but the same cannot be said for BCPE or BCT distributions.

Entry of basic demographic information (sex, date of birth, and scan date) and one or more HR-pQCT outcome into the Excel calculators (Fig. 1A) results in plotting of sex-specific centile curves and computation of subject-specific percentiles, z-scores, and t-scores (Fig. 1B). For Ct.Po, Ct.Po.Dm, and Tb.Sp higher values were considered less desirable and, thus, yield lower z- and t-scores. Representative images of reconstructed and segmented scans in females and males are provided in Figs. 2 and 3, respectively.

Centile curves at distal bone sites

Centile curves for Tt.vBMD, Tb.BV/TV, Tb.Th, and failure load (using Pistoia criteria) are presented for the distal radius (Fig. 4) and tibia (Fig. 5). Centile curves for other outcomes, including failure load estimated using Arias-Morena criteria, are provided in Supplemental files 4 (distal radius) and 5 (distal tibia). For most measures, the fitted median centile curve was highest at the youngest age in the cohort. Exceptions at the distal radius were Tt.vBMD (peak at 35.3 and 31.8 years in females and males, respectively), Ct.vBMD (peak at 41.3 and 35.9 years in females and males, respectively), Tt.Ar (peak at maximum database age in males [80.0 years]), Ct.Ar (peak at 39.8 years in males), Tb.Ar (peak at maximum age in females [79.9 years] and males [80.0 years]), and Tb.Th (peak at maximum age in females [79.9 years]). Exceptions at the distal tibia were Ct.vBMD (peak at 36.3 and 33.2 years in females and males, respectively), Tt.Ar (peak at maximum age in females [79.9 years] and males [80.0 years]), Ct.Ar (peak at 30.1 years and 44.1 years in females and males, respectively), Tb.Ar (peak at maximum age in females [79.9 years] and males [80.0 years]), Ct.Th (peak at 35.8 years in females), and Tb.Th (peak at maximum age [79.9 years] in females).

Centile curves at diaphyseal bone sites

Centile curves for Ct.vBMD, Ct.Th, Ct.Po, and failure load (using Pistoia criteria) are presented for the radial (Fig. 6) and tibial (Fig. 7) diaphysis. Centile curves for other outcomes, including failure load estimated using Arias-Morena criteria, are provided in Supplemental files 6 (radial diaphysis) and 7 (tibial diaphysis). The fitted median centile curve was highest at varying ages depending on the specific HR-pQCT outcome. Peak Ct.vBMD values occurred in females and males aged 36.9 to 46.5 yrs at both the radial and tibial diaphysis. Tt.Ar at the radial diaphysis in females and males was greatest at the maximum age in the database. Tibial diaphysis Tt.Ar in males was also greatest at the maximum database age. Ct.Ar, Ct.Th, stiffness, and failure load at the
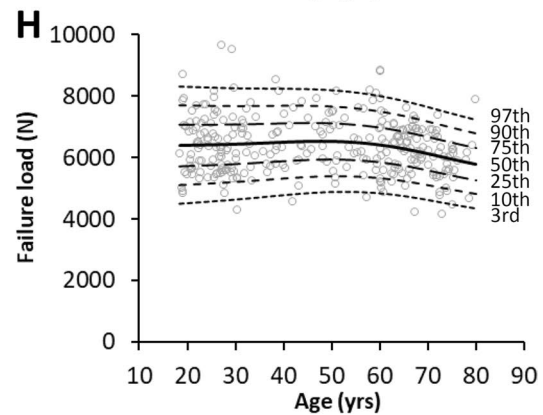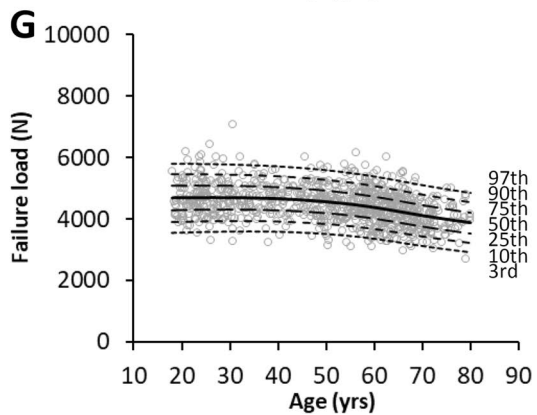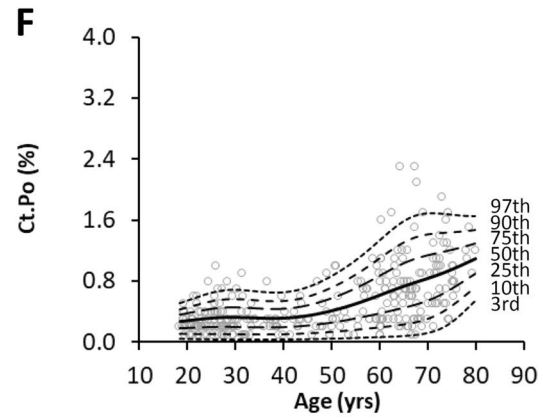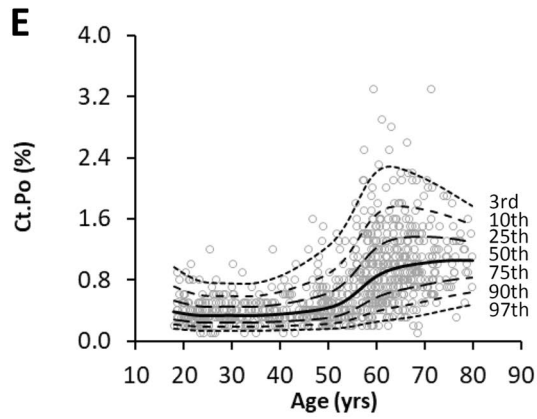
RADIAL DIAPHYSIS
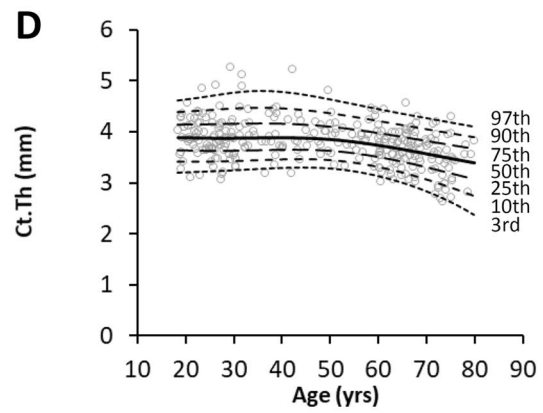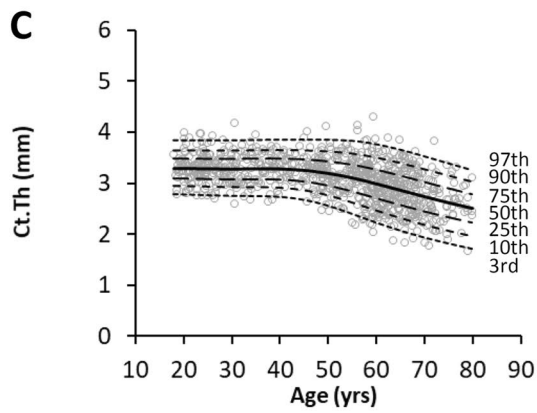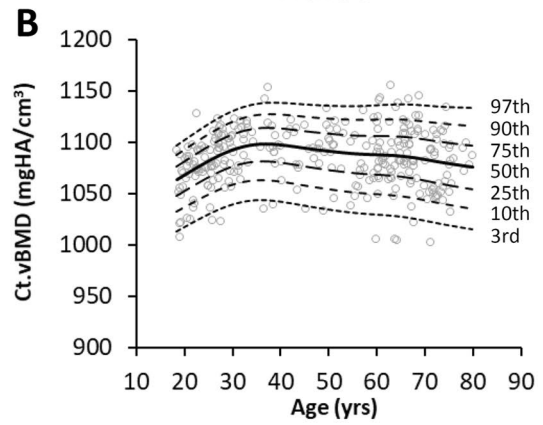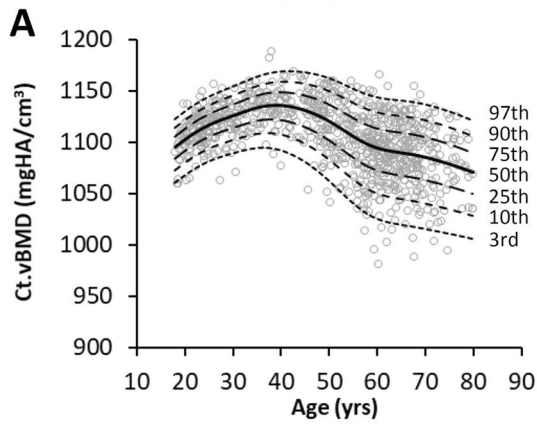
radial and tibial diaphysis had highest values in females and males aged < 50 years. Ct.Po at both the radial and tibial diaphysis was low in females and males aged < 50 years and increased thereafter.

Impact of criteria on failure load

There was a strong linear relationship ($R^2 > 0.99$) between failure load estimated using Pistoia [24] and Arias-Morena [25] criteria (all $P < 0.001$). Site-specific regression equations to convert estimated failure load using the different criteria are:

Distal radius Arias-Morena failure load = 1.581 ∗ Pistoia failure load + 170.24

Radial diaphysis Arias-Morena failure load = 1.526 ∗ Pistoia failure load − 59.12

Distal tibia Arias-Morena failure load = 1.589 ∗ Pistoia failure load − 2.91

Tibial diaphysis Arias-Morena failure load = 1.555 ∗ Pistoia failure load − 164.17

Discussion

The current study provides unique data and resources which complement and further recently published HR-pQCT reference datasets. The unique data include the generation of reference data: (1) at anatomically standardized regions; (2) using a second-generation HR-pQCT scanner; and (3) at diaphyseal (in addition to distal) bone locations. The unique resources are the: (1) generation of regression equations to convert between µFE-estimated failure load using the original Pistoia [24] and newer Arias-Morena [25] criteria and (2) development of practical Excel-based calculators (Supplemental files 1 and 2) based on the normative curves fitted using the LMS approach. The regression equations enable conversion and cross-study comparisons of data acquired using the two sets of failure load criteria. The Excel-based calculators can plot an individual's outcomes on the centile curves presented here and compute subject-specific percentiles, z-scores, and t-scores.

The generation of reference data at anatomically standardized regions by using percent-of-length offsets is novel. To our knowledge, percent-of-length offsets have only been used once previously to generate HR-pQCT reference data,

with the data limited to distal bone sites in adolescents and young adults and acquired using a first-generation scanner [8]. Recent HR-pQCT guidelines recommend the field transition from performing HR-pQCT scans at conventional fixed offsets to using percent-of-length offsets [23]. A percent-of-length offset controls for differences in bone length which can result in inclusion of differing proportions of cortical and trabecular bone when using fixed offsets [19–21]. The latter may lead to the generation of imprecise percentiles and z- and t-scores which may be important when determining bone status within an individual or population of interest.

The distal scan sites in the current cohort (4% distal radius and 7.3% distal tibia) were chosen as, on average, they reportedly approximate the scan locations while using fixed offsets [19, 23]. If scan locations when using percent-of-length and fixed offsets do generally approximate, centile curves and peak median values on the population level should be similar when using the two different offset approaches. However, there are noticeable differences when comparing our distal radius data to those reported by Whittier et al. [15] who also used a second-generation HR-pQCT scanner to generate reference data in a mostly White population.

Peak median values in young adults for distal radius Ct.vBMD, Tb.vBMD, and trabecular microarchitectural outcomes (Tb.BV/TV, Tb.N, Tb.Th, Tb.Sp) are similar (< 5% difference) between the current study and that of Whittier et al. [15]. However, both females and males in our cohort had ~ 15% lower distal radius Tt.vBMD with ~ 17% greater Tt.Ar, ~ 30% greater Tb.Ar, and more than 10% lower Ct.Th. These differences are consistent with systemically scanning a more distal location in the current cohort, with the distal radius increasing in cross-sectional size and its cortex thinning as you move distally [22].

One reason for a systemic difference in scanning location may be related to subtleties associated with using a different reference line location. We placed our reference line at the medial edge of the distal radius articular surface (as recommended when using percent-of-length offsets [23]), as opposed to the more distal central ridge between the scaphoid and lunate fossae typically used with a fixed offset. A 4% offset from our reference line location corresponded with
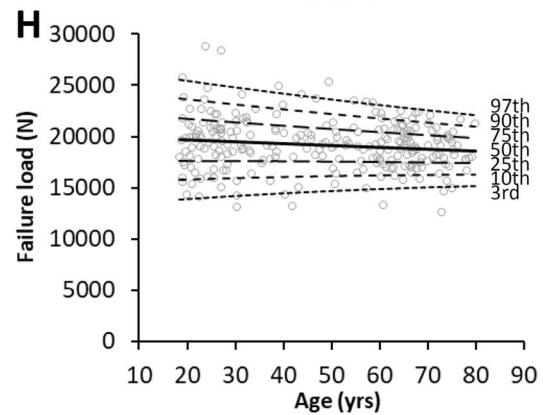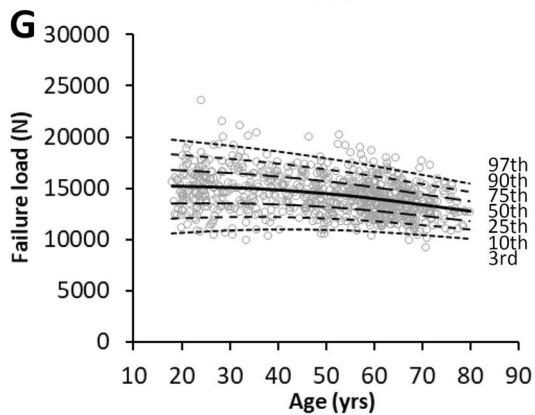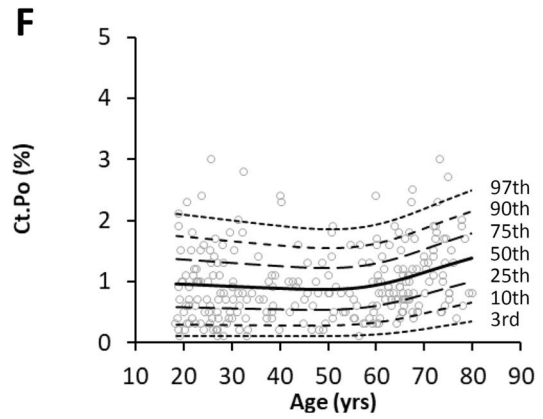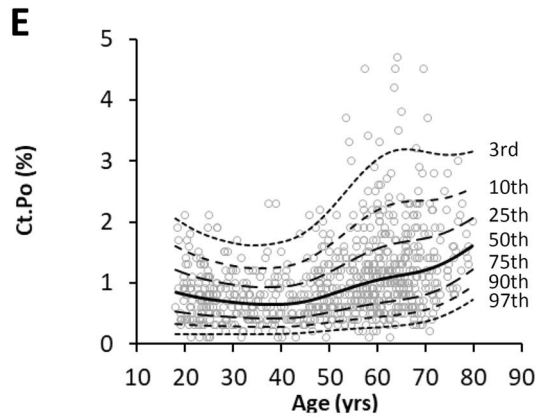
TIBIAL DIAPHYSIS

Females   Males
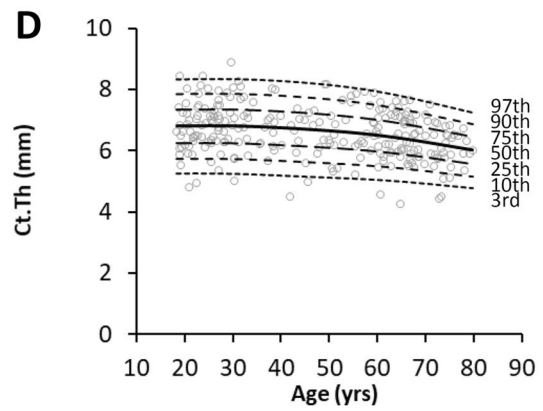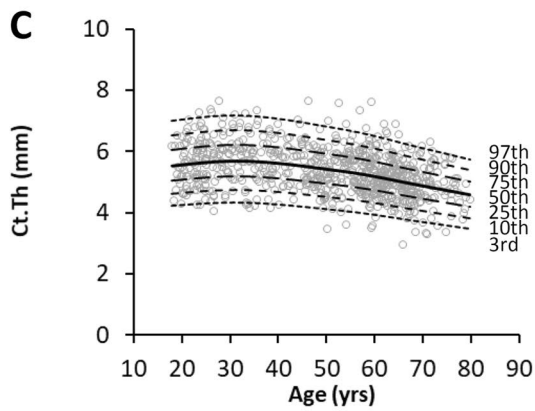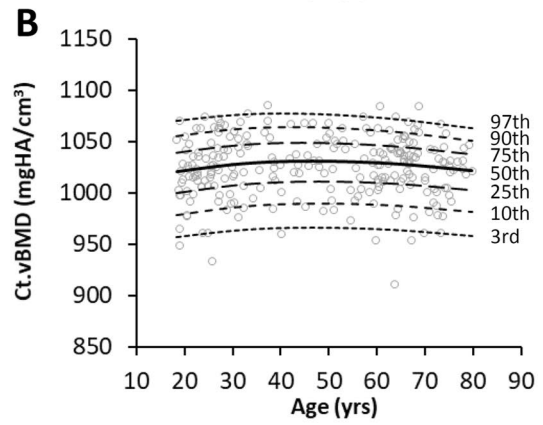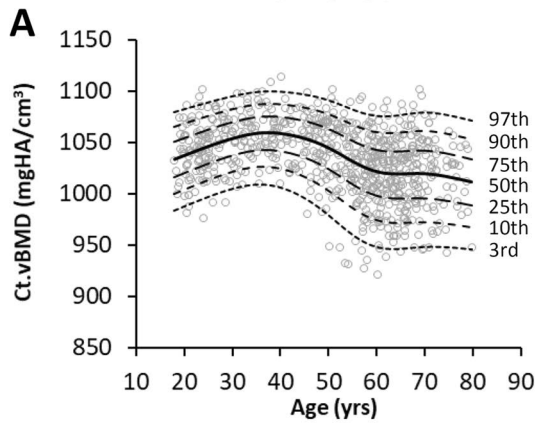
average fixed offsets of 5.1 mm (IQR = 4.7–5.4 mm) and 6.1 mm (IQR = 5.7–6.6 mm) in females and males, respectively. These locations may not accurately correspond with that when scanning 9.0 mm proximal from the more distal reference line placed when using the fixed offset approach.

In comparison to at the distal radius, reference line positioning at the distal tibia is consistent when using either a percent-of-length or fixed offset allowing for better assessment of comparability. A 7.3% offset in our cohort corresponded with an average offset of 21.7 mm (IQR = 20.6–22.7 mm) and 24.1 mm (IQR = 22.8–25.6 mm) in females and males, respectively. The average offset in females approximates the 22.0 mm offset typically used when scanning with a fixed offset approach when using second-generation HR-pQCT. Accordingly, peak median values at the distal tibia in younger females in the current study and that of Whittier et al. [15] are strikingly similar. However, the larger average offset in males in the current study highlights the limitation of using fixed offsets.

Using the conventional 22.0 mm fixed offset in males would have, on average, shifted scan location distally approximately 20% (2.1 mm) of total scan length (10.2 mm) because of the longer bone lengths in our male participants. While the rate of change of bone properties at the distal tibia is lower than that at the distal radius [22], comparing the current data to that reported by Whittier et al. [15] suggests that the later study did indeed scan a more distal location in males. In particular, Whittier et al. [15] reported peak median outcomes at the distal tibia in younger males that were larger for Tt.Ar, and lower for Tt.vBMD (~5%), Ct.Ar (~15%), and Ct.Th (~13%) than in the current study.

Peak median values (using the Pistoria failure criteria [24]) for estimated failure load in younger adults in the current study were ~15–20% and ~25–30% higher at the distal radius and tibia, respectively. In addition to the aforementioned potential differences in scanning location and subsequent density and morphological outcomes, a reason for our higher peak median values for estimated failure load is our use of a higher modulus (10 GPa vs. 8.7 GPa). A higher modulus linearly increases estimated failure load [35].

The centile curves generated with the current cross-sectional data allow for comparisons between ages, sexes, and sites and affirm previous observations regarding bone changes with aging. At each site and in both sexes, the fitted median centile curve for Ct.vBMD progressively increased between ages 18 and ~40 years before declining thereafter. The decline was more precipitous in females at both the distal and diaphyseal sites and was coupled with a transition in the rate of centile curve change of median Ct.Po in females

aged 50–60 years—likely corresponding with changes associated with perimenopause. Fitted median centile curves for Ct.Ar and Ct.Th progressively declined with age in females at all sites. As Tt.Ar remained relatively constant, the decline in cortical properties in females most likely occurred near the cortical/trabecular transitional zone. These changes in cortical bone properties were tempered in males.

Preferential loss of bone near the cortical/trabecular bone transition may explain some of the trabecular observations in females with age. In particular, the fitted median centile curve for Tb.Th at both the distal radius and tibia in females began to increase after reaching a nadir around 50 years of age. The apparent increase in thickness may be due to our inclusion of a relatively lower number of older adults who may have been on the healthier end of the bone health spectrum. LMS curves are sensitive to individuals at the tails of the distribution. However, the hypothesis of higher than average bone health in our older females is not supported by the curves for Tt.vBMD and estimated failure load which continued to decline with age, and the observation that females aged 70–80 years in our cohort had an average total hip aBMD t-score in the osteopenic range (mean ± SD = − 1.1 ± 0.8).

An increase in Tb.Th at the distal radius with age in females has been shown in a previous prospective HR-pQCT study [36] and is likely due to trabecularization of cortical bone adjacent to the trabecular compartment. Endochondral resorption and intracortical remodeling during aging leaves cortical bone fragments in the cortical/trabecular transitional zone [37]. As the standard HR-pQCT image-processing algorithm automatically segments cortical and trabecular bone based on density thresholds, cortical remnants present in older individuals can be assigned to the trabecular compartment resulting in the underestimation of trabecular and overestimation of cortical bone changes [38]. In our case, the result was a rise in the fitted median curve for Tb.Th in older females at distal sites coupled with an apparent reduction in the decline of the fitted median curves for Tb.vBMD and Tb.BV/TV.

The assignment of cortical bone fragments to the trabecular compartment possibly also contributes to the pattern of change in Ct.vBMD at the diaphyseal sites. As mentioned above, there was a transition to a larger rate of median Ct.vBMD loss at diaphyseal sites after reaching a peak at age 40 years. This was followed by a second transition in the rate of median curve change around 60 years of age wherein Ct.vBMD loss appeared to plateau with increasing age. The reduction in Ct.vBMD loss beyond 60 years may be due to slowing of menopause-related changes. Alternatively, it may be due to bone loss in the cortical/trabecular transitional zone resulting in a greater proportion of lower-density cortical remnants being counted as trabecular bone. The net result is an apparent reduction in the loss of Ct.vBMD.

HR-pQCT provides the ability to separate the cortical and trabecular compartments; however, parameters potentially influenced by transitional zone changes require careful interpretation. In particular, t-scores for parameters that showed an apparent reversal in trends with increasing age (e.g., Tb.vBMD, Tb.BV/TV, and Tb.Th at the distal radius and Tb.Th at the distal tibia in females) may not be useful for detailing an individual's bone status (in fact, t-scores for Tb.Th at distal sites in females are not calculatable as the peak on the fitted median curves occurred at the oldest age in the dataset). Instead, it may be that whole bone parameters (e.g., Tt.vBMD, stiffness, estimated failure load) provide the most robust outcomes for assessing general bone status, particularly at distal skeletal sites. Supporting this, estimated failure load at distal sites has been found to have the greatest association with the risk of fracture [2]. The utility of estimated mechanical properties at diaphyseal sites remains to be established as the µFE models utilize axial or uniaxial compressive loads, whereas resistance to bending will also be relevant at diaphyseal sites.

Our study has a number of strengths, including the development of reference data for second-generation HR-pQCT scans at distal and diaphyseal sites in a self-reported racially homogenous population. However, our study is not without limitations. Data were obtained at a single center and variability in machine performance at other centers may influence outcomes and percentiles. Our normative curves were generated using cross-sectional data, which may not represent an individual's trajectory over time [39]. We used the HR-pQCT manufacturer's standard software to segment bones and did not use alternative segmentation approaches (e.g., StrAx software [40]) to potentially improve localization of the cortical/trabecular transitional zone. We did not assess the appropriateness of our sample size and sample composition, as recently recommended by Cole [34]. It remains unclear whether the regions assessed correspond with where fractures occur clinically, particularly at the distal radius [41]. Finally, we had more limited inclusion of males and older (age > 70 years) adults, our data are specific to White individuals living in the Midwest of the United States, and we did not collect data on medication use (beyond excluding those currently taking bone active therapies).

In summary, the current study provides age- and sex-specific normative data for HR-pQCT measures of the distal and diaphyseal radius and tibia acquired using percent-of-length offsets. The generated centile curves and calculators enable HR-pQCT outcomes in an individual or population of interest to be expressed relative to the reference cohort. Comparison to a reference cohort can be of benefit as it can negate the need to establish a control group in cross-sectional studies and can indicate the magnitude of difference from expected values. However, careful consideration needs to be given to the suitability of the reference population in terms of race and ethnicity, age, sex, and other demographic characteristics. Also, consideration needs to be given to the HR-pQCT scanning and analysis procedures utilized, including how limb lengths are measured and where reference lines are placed. Ultimately, the expectation is that these data will be expanded over time and the wealth of information HR-pQCT provides becomes increasingly interpretable and utilized.

Declarations

Ethics approval Institutional Review Board approval was obtained from Indiana University.

Conflict of interest Bert van Rietbergen is a consultant for Scanco Medical AG. Stuart Warden, Ziyue Liu, Robyn Fuchs, and Sharon Moe declare that they have no conflict of interest.

References

1. Mikolajewicz N, Bishop N, Burghardt AJ, Folkestad L, Hall A, Kozloff KM et al (2020) HR-pQCT measures of bone microarchitecture predict fracture: systematic review and meta-analysis. J Bone Miner Res 35(3):446–459. https://doi.org/10.1002/jbmr.3901

2. Samelson EJ, Broe KE, Xu H, Yang L, Boyd S, Biver E et al (2019) Cortical and trabecular bone microarchitecture as an independent predictor of incident fracture risk in older women and men in the bone microarchitecture international consortium (BoMIC): a prospective study. Lancet Diabetes Endocrinol 7(1):34–43. https://doi.org/10.1016/s2213-8587(18)30308-5

3. Alvarenga JC, Fuller H, Pasoto SG, Pereira RM (2017) Age-related reference curves of volumetric bone density, structure, and biomechanical parameters adjusted for weight and height in a population of healthy women: an HR-pQCT study. Osteoporos Int 28(4):1335–1346. https://doi.org/10.1007/s00198-016-3876-0

4. Burghardt AJ, Kazakia GJ, Ramachandran S, Link TM, Majumdar S (2010) Age- and gender-related differences in the geometric properties and biomechanical significance of intracortical porosity in the distal radius and tibia. J Bone Miner Res 25(5):983–993. https://doi.org/10.1359/jbmr.091104

5. Burt LA, Liang Z, Sajobi TT, Hanley DA, Boyd SK (2016) Sex- and site-specific normative data curves for HR-pQCT. J Bone Miner Res 31(11):2041–2047. https://doi.org/10.1002/jbmr.2873

6. Burt LA, Macdonald HM, Hanley DA, Boyd SK (2014) Bone microarchitecture and strength of the radius and tibia in a reference population of young adults: an HR-pQCT study. Arch Osteoporos 9:183. https://doi.org/10.1007/s11657-014-0183-2

7. Dalzell N, Kaptoge S, Morris N, Berthier A, Koller B, Braak L et al (2009) Bone micro-architecture and determinants of strength in the radius and tibia: age-related changes in a population-based study of normal adults measured with high-resolution pQCT. Osteoporos Int 20(10):1683–1694. https://doi.org/10.1007/s00198-008-0833-6

8. Gabel L, Macdonald HM, Nettlefold LA, McKay HA (2018) Sex-, ethnic-, and age-specific centile curves for pQCT- and HR-pQCT-derived measures of bone structure and strength in adolescents and young adults. J Bone Miner Res 33(6):987–1000. https://doi.org/10.1002/jbmr.3399

9. Hansen S, Shanbhogue V, Folkestad L, Nielsen MM, Brixen K (2014) Bone microarchitecture and estimated strength in 499 adult Danish women and men: a cross-sectional, population-based high-resolution peripheral quantitative computed tomographic study on peak bone structure. Calcif Tissue Int 94(3):269–281. https://doi.org/10.1007/s00223-013-9808-5

10. Hung VW, Zhu TY, Cheung WH, Fong TN, Yu FW, Hung LK et al (2015) Age-related differences in volumetric bone mineral density, microarchitecture, and bone strength of distal radius and tibia in Chinese women: a high-resolution pQCT reference database study. Osteoporos Int 26(6):1691–1703. https://doi.org/10.1007/s00198-015-3045-x

11. Khosla S, Riggs BL, Atkinson EJ, Oberg AL, McDaniel LJ, Holets M et al (2006) Effects of sex and age on bone microstructure at the ultradistal radius: a population-based noninvasive in vivo assessment. J Bone Miner Res 21(1):124–131. https://doi.org/10.1359/jbmr.050916

12. Macdonald HM, Nishiyama KK, Kang J, Hanley DA, Boyd SK (2011) Age-related patterns of trabecular and cortical bone loss differ between sexes and skeletal sites: a population-based HR-pQCT study. J Bone Miner Res 26(1):50–62. https://doi.org/10.1002/jbmr.171

13. Stuck AK, Schenk D, Zysset P, Bütikofer L, Mathis A, Lippuner K (2020) Reference values and clinical predictors of bone strength for HR-pQCT-based distal radius and tibia strength assessments in women and men. Osteoporos Int 31(10):1913–1923. https://doi.org/10.1007/s00198-020-05405-0

14. Vilayphiou N, Boutroy S, Sornay-Rendu E, Van Rietbergen B, Chapurlat R (2016) Age-related changes in bone strength from HR-pQCT derived microarchitectural parameters with an emphasis on the role of cortical porosity. Bone 83:233–240. https://doi.org/10.1016/j.bone.2015.10.012

15. Whittier DE, Burt LA, Hanley DA, Boyd SK (2020) Sex- and site-specific reference data for bone microarchitecture in adults measured using second-generation HR-pQCT. J Bone Miner Res 35(11):2151–2158. https://doi.org/10.1002/jbmr.4114

16. Yu F, Xu Y, Hou Y, Lin Y, Jiajue R, Jiang Y et al (2020) Age-, site-, and sex-specific normative centile curves for HR-pQCT-derived microarchitectural and bone strength parameters in a Chinese mainland population. J Bone Miner Res 35(11):2159–2170. https://doi.org/10.1002/jbmr.4116

17. Zhu TY, Yip BH, Hung VW, Choy CW, Cheng KL, Kwok TC et al (2018) Normative standards for HRpQCT parameters in Chinese men and women. J Bone Miner Res 33(10):1889–1899. https://doi.org/10.1002/jbmr.3481

18. Manske SL, Zhu Y, Sandino C, Boyd SK (2015) Human trabecular bone microarchitecture can be assessed independently of density with second generation HR-pQCT. Bone 79:213–221. https://doi.org/10.1016/j.bone.2015.06.006

19. Bonaretti S, Majumdar S, Lang TF, Khosla S, Burghardt AJ (2017) The comparability of HR-pQCT bone measurements is improved by scanning anatomically standardized regions. Osteoporos Int 28(7):2115–2128. https://doi.org/10.1007/s00198-017-4010-7

20. Ghasem-Zadeh A, Burghardt A, Wang XF, Iuliano S, Bonaretti S, Bui M et al (2017) Quantifying sex, race, and age specific differences in bone microstructure requires measurement of anatomically equivalent regions. Bone 101:206–213. https://doi.org/10.1016/j.bone.2017.05.010

21. Shanbhogue VV, Hansen S, Halekoh U, Brixen K (2015) Use of relative vs fixed offset distance to define region of interest at the distal radius and tibia in high-resolution peripheral quantitative computed tomography. J Clin Densitom 18(2):217–225. https://doi.org/10.1016/j.jocd.2014.12.002

22. Boyd SK (2008) Site-specific variation of bone micro-architecture in the distal radius and tibia. J Clin Densitom 11(3):424–430. https://doi.org/10.1016/j.jocd.2007.12.013

23. Whittier DE, Boyd SK, Burghardt AJ, Paccou J, Ghasem-Zadeh A, Chapurlat R et al (2020) Guidelines for the assessment of bone density and microarchitecture in vivo using high-resolution peripheral quantitative computed tomography. Osteoporos Int 31(9):1607–1627. https://doi.org/10.1007/s00198-020-05438-5

24. Pistoia W, van Rietbergen B, Lochmuller EM, Lill CA, Eckstein F, Ruegsegger P (2002) Estimation of distal radius failure load with micro-finite element analysis models based on three-dimensional peripheral quantitative computed tomography images. Bone 30(6):842–848

25. Arias-Moreno AJ, Hosseini HS, Bevers M, Ito K, Zysset P, van Rietbergen B (2019) Validation of distal radius failure load predictions by homogenized- and micro-finite element analyses based on second-generation high-resolution peripheral quantitative CT images. Osteoporos Int 30(7):1433–1443. https://doi.org/10.1007/s00198-019-04935-6

26. van den Bergh JP, Szulc P, Cheung AM, Bouxsein M, Engelke K, Chapurlat R (2021) The clinical application of high-resolution peripheral computed tomography (HR-pQCT) in adults: state of the art and future directions. Osteoporos Int. https://doi.org/10.1007/s00198-021-05999-z

27. Auerbach BM, Ruff CB (2006) Limb bone bilateral asymmetry: variability and commonality among modern humans. J Hum Evol 50(2):203–218. https://doi.org/10.1016/j.jhevol.2005.09.004

28. Peters M (1988) Footedness: asymmetries in foot preference and skill and neuropsychological assessment of foot movement. Psychol Bull 103(2):179–192. https://doi.org/10.1037/0033-2909.103.2.179

29. Warden SJ, Wright CS, Fuchs RK (2021) Bone microarchitecture and strength adaptation to physical activity: a within-subject controlled. HRpQCT study. Med Sci Sports Exerc 53(6):1179–1187. https://doi.org/10.1249/MSS.0000000000002571

30. Sode M, Burghardt AJ, Pialat JB, Link TM, Majumdar S (2011) Quantitative characterization of subject motion in HR-pQCT images of the distal radius and tibia. Bone 48(6):1291–1297. https://doi.org/10.1016/j.bone.2011.03.755

31. Cole TJ, Green PJ (1992) Smoothing reference centile curves: the LMS method and penalized likelihood. Stat Med 11(10):1305–1319. https://doi.org/10.1002/sim.4780111005

32. Rigby RA, Stasinopoulos DM (2005) Generalized additive models for location, scale and shape. J Roy Stat Soc Ser C (Appl Stat) 54(3):507–554. https://doi.org/10.1111/j.1467-9876.2005.00510.x

33. Centers for Disease Control and Prevention. Modified z-scores in the CDC growth charts. https://www.cdc.gov/nccdphp/dnpa/growthcharts/resources/biv-cutoffs.pdf. Accessed Mar 5 2021

34. Cole TJ (2021) Sample size and sample composition for constructing growth reference centiles. Stat Methods Med Res 30(2):488–507. https://doi.org/10.1177/0962280220958438

35. Whittier DE, Manske SL, Kiel DP, Bouxsein M, Boyd SK (2018) Harmonizing finite element modelling for non-invasive strength estimation by high-resolution peripheral quantitative computed tomography. J Biomech 80:63–71. https://doi.org/10.1016/j.jbiomech.2018.08.030

36. Kawalilak CE, Johnston JD, Olszynski WP, Kontulainen SA (2014) Characterizing microarchitectural changes at the distal radius and tibia in postmenopausal women using HR-pQCT. Osteoporos Int 25(8):2057–2066. https://doi.org/10.1007/s00198-014-2719-0

37. Zebaze RMD, Ghasem-Zadeh A, Bohte A, Iuliano-Burns S, Mirams M, Price RI et al (2010) Intracortical remodelling and porosity in the distal radius and post-mortem femurs of women: a cross-sectional study. Lancet 375(9727):1729–1736. https://doi.org/10.1016/S0140-6736(10)60320-0

38. Zebaze R, Seeman E (2015) Cortical bone: a challenging geography. J Bone Miner Res 30(1):24–29. https://doi.org/10.1002/jbmr.2419

39. Burt LA, Hanley DA, Boyd SK (2017) Cross-sectional versus longitudinal change in a prospective HR-pQCT study. J Bone Miner Res 32(7):1505–1513. https://doi.org/10.1002/jbmr.3129

40. Zebaze R, Ghasem-Zadeh A, Mbala A, Seeman E (2013) A new method of segmentation of compact-appearing, transitional and trabecular compartments and quantification of cortical porosity from high resolution peripheral quantitative computed tomographic images. Bone 54(1):8–20. https://doi.org/10.1016/j.bone.2013.01.007

41. Baumbach SF, Schmidt R, Varga P, Heinz T, Vécsei V, Zysset PK (2011) Where is the distal fracture line location of dorsally displaced distal radius fractures? J Orthop Res 29(4):489–494. https://doi.org/10.1002/jor.21268

Publisher's note Springer Nature remains neutral with regard to jurisdictional claims in published maps and institutional affiliations.